Preferential Location of Dopants in the Amorphous Phase of Oriented Regioregular Poly(3-hexylthiophene-2,5-diyl) Films Helps Reach Charge Conductivities of 3000 S cm −1

Yuhan Zhong, Viktoriia Untilova, Dominique Muller, Shubhradip Guchait, Céline Kiefer, Laurent Herrmann, Nicolas Zimmermann, Marion Brosset, Thomas Heiser, Martin Brinkmann

Preferential location of dopants in the amorphous phase of oriented regioregular poly(3-hexylthiophene-2,5-diyl) films helps reach charge conductivities of 3000 S/cm.

Yuhan Zhong[1,2], Viktoriia Untilova[1], Dominique Muller[2], Shubhradip Guchait[1], Céline Kiefer[3], Laurent Herrmann[1], Nicolas Zimmermann[2], Marion Brosset[1], Thomas Heiser[2], Martin Brinkmann[1*]

(1) Université de Strasbourg, CNRS, ICS UPR 22, F-67000 Strasbourg, France

(2) Université de Strasbourg, CNRS ENGEES, INSA, ICUBE UMR 7357, F-67000, Strasbourg, France

(3) Université de Strasbourg, CNRS, IPCMS UMR 7504, F-67087 Strasbourg, France

* corresponding author : martin.brinkmann@ics-cnrs.unistra.fr

Abstract

Doping polymer semiconductors is a central topic in plastic electronics and especially in the design of novel thermoelectric materials. In this contribution, we demonstrate that doping of oriented semi-crystalline P3HT thin films with the dopant tris(4-bromophenyl)ammoniumyl hexachloroantimonate), known as magic blue (MB), helps reach charge conductivities of 3000 S/cm and thermoelectric power factors of 170±30 $\mu W/mK^2$ along the polymer chain direction. A combination of transmission electron microscopy, polarized optical absorption spectroscopy, Rutherford backscattering and thermoelectric property measurements helps clarify the conditions necessary to achieve such high charge conductivities. A comparative study with different dopants demonstrates that the doping mechanism is intimately related to the semi-crystalline structure of the polymer and whether crystalline, amorphous or both phases are doped. The highest charge mobilities are observed when the dopant MB is preferentially located in the amorphous phase of P3HT, leaving the structure of P3HT nanocrystals almost unaltered. In this case, the P3HT nanocrystals are doped from their interface with the surrounding amorphous phase. These results indicate that doping preferentially the amorphous phase of semi-crystalline polymer semiconductors is an effective strategy to reduce polaron localization, enhance charge mobilities and improve thermoelectric power factors.

I. Introduction.

Polymer semiconductors such as regio-regular poly(3-hexylthiophene) (P3HT) or Poly[2,5-bis(3-alkylthiophen-2-yl)thieno[3,2-*b*]thiophene] (PBTTTs) are of high interest to the community of plastic electronics for their remarkable opto-electronic properties and ease of processing. [1,2,3] Depending on the charge carrier density, these polythiophenes can show either semi-conducting properties of interest for the design of organic Field Effect Transistors (OFETs) or metallic-like charge transport that is essential when using such polymers as charge transporting layers in organic solar cells. [3] In the last decade, doped polymer semiconductors emerged as promising materials for thermoelectric applications.[4-5] Doping is a general method to tune the charge carrier density in polymers.[6] It can be achieved in different ways e.g. via electrochemistry by oxidizing/reducing a polymer layer atop an electrode[7-9] or by redox doping with strong acceptor molecules such as 2,3,5,6-Tetrafluoro-7,7,8,8-tetracyanoquinodimethane (F_4TCNQ).[10-15] Understanding of the correlations between the microstructure of the doped polymers and their thermoelectric (TE) properties is central in the optimization path of thermoelectric organic materials. So far, detailed studies on structure-TE property correlations were investigated for polythiophenes doped with F_4TCNQ, F_6TCNNQ[16-19] $FeCl_3$[20] and Mo(tdf-$COCF_3$)$_3$.[21-23] Generally speaking, the studies of doping of polymer semiconductors such as P3HT and PBTTT have demonstrated the key role of the following parameters: i) dopant's electron affinity[21], ii) the method of doping (sequential *versus* direct doping from solution, vapor phase *versus* solution doping)[15,24,25], iii) the structure of the pristine polymer prior to doping[26,27] and iv) the structure of alkyl side chain layers that host the dopant molecules.[28,29] For p-type polymer semiconductors, effective doping implies to fine-tune the position of the polymer's Highest Occupied Molecular Orbital

(HOMO) level with respect to the Lowest Unoccupied Molecular Orbital (LUMO) of the dopant. Therefore, in order to be able to dope alternated donor-acceptor copolymers such as PDPP-3T that have a deep HOMO level, it is of importance to use dopants with higher electron affinity. The following p-type dopants show increasing electronic affinity (EA): F_4TCNQ (5.2 eV), F_6TCNNQ (5.37 eV[16-18]), $Mo(tdf\text{-}COCF_3)_3$ (5.5 eV[21-23]) and finally MB (5.8 eV[30]) (see Figure 1). Recent results on doping of oriented semi-crystalline P3HT have also shown that EA of the dopant controls the possibility to dope the crystalline or amorphous fractions of the polymer.[31] Indeed, like most polymer semi-conductors, rr-P3HT shows a characteristic semi-crystalline morphology, particularly well observed in thin films oriented by epitaxy or high-temperature rubbing (HTR). [32,33] In such oriented films, TEM reveals a periodic lamellar morphology where crystalline lamellae alternate with amorphous interlamellar zones. Most importantly, the temperature at which such films are aligned by HTR is a means to tune the lamellar periodicity and the extension of crystalline domains. [33] F_4TCNQ and F_6TCNNQ have been shown to dope little the amorphous phase of P3HT since it has a deeper HOMO than the crystalline domains.[19] In strong contrast, dopants such as $FeCl_3$ or $Mo(tdf\text{-}COCF_3)_3$ are able to dope both crystalline and amorphous domains of P3HT and this leads to larger charge conductivities than for F_4TCNQ and F_6TCNNQ.[23] Accordingly, it is important to determine to what extent the dopant's EA can influence the mechanism of doping of a semi-crystalline polymer such as P3HT since the final TE performances must correlate to the amount and location of dopants in the semi-crystalline matrix of the polymer. So far, detailed studies on structure-TE property correlations were performed for oriented P3HT films doped with F_4TCNQ, $FeCl_3$, F_6TCNNQ and $Mo(tdf\text{-}COCF_3)_3$. Record TE power factors of 160 $\mu W/mK^2$ were reported for aligned P3HT films doped with $Mo(tdf\text{-}COCF_3)_3$.[23]

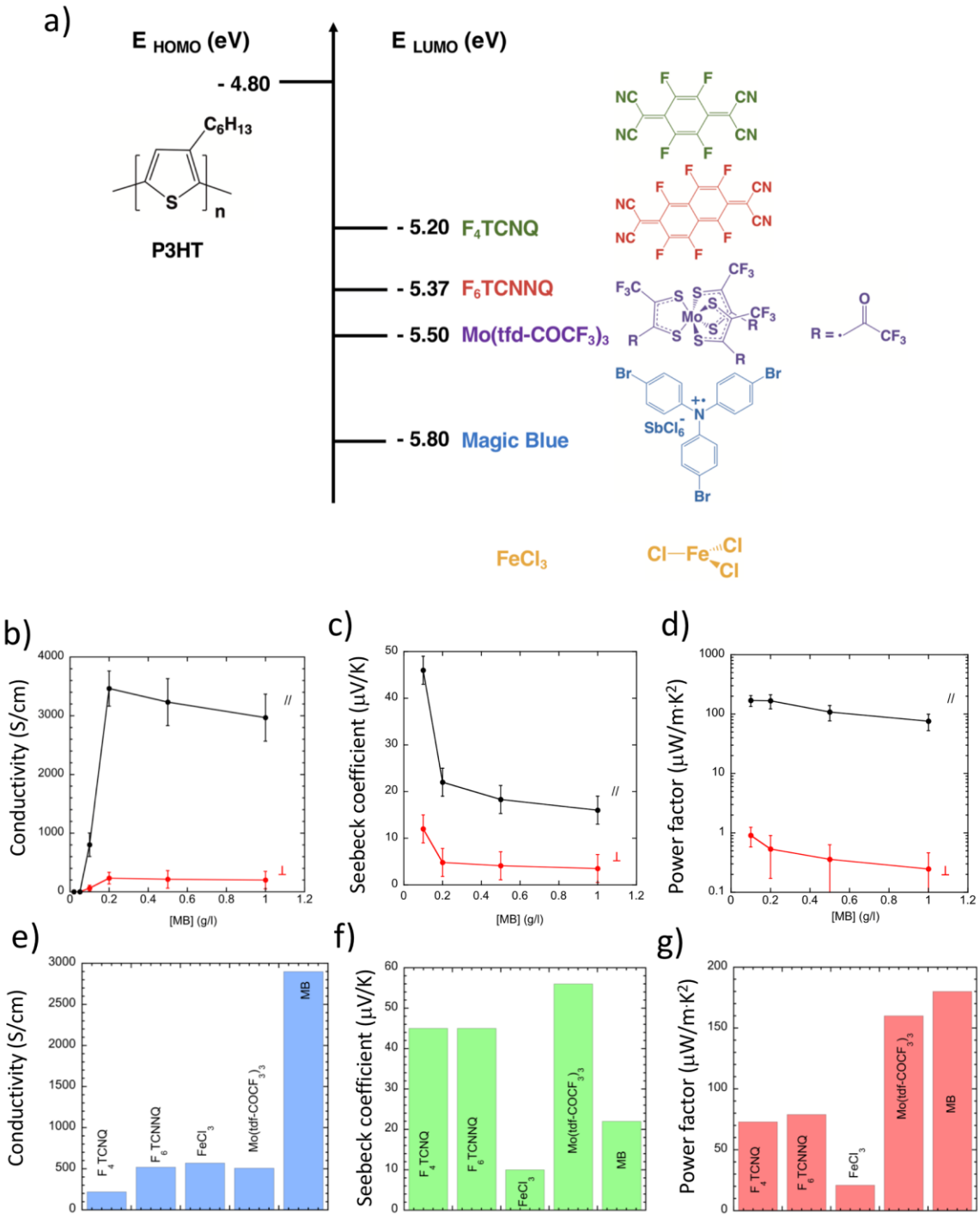

Figure 1. a) Molecular structure and positions of the LUMO of the dopants with respect to the HOMO of P3HT. Evolution of the charge conductivity (b), the Seebeck coefficient (c) and of the thermoelectric power factor (d) of oriented P3HT thin films doped with magic blue as measured in the directions parallel (red dots) and perpendicular (black dots). The film thickness was 38nm. e)-g) Maximum values of the charge conductivity $\sigma_{//}$, the Seebeck

coefficient $S_{//}$ and the power factor $PF_{//}$ measured in the direction parallel to the polymer chains in rubbed thin films of P3HT doped with different dopants.

In this contribution, we focus on the dopant tris(4-bromophenyl)ammoniumyl hexachloroantimonate , also known as Magic blue (MB). MB is a strong oxidant able to dope homopolymers such as P3HT as well as high mobility alternated Donor-Acceptor copolymers such as PDPP-3T.[30] In the case of P3HT, doping non-oriented films with MB in ambient conditions leads to electrical conductivities up to 26 S/cm.[30] In the redox reaction between P3HT and MB, electron transfer from the polymer to the tris(bromophenyl)ammoniumyl radical cation of MB yields a neutral and spinless molecule of tris(4-bromophenyl)amine that is transparent in the UV-vis range. In this doping process, $SbCl_6^-$ serves as the counterion for the doped P3HT and is thus expected to be incorporated to some extent inside the polymer matrix.

We first investigate in detail the doping mechanism of P3HT films with MB. In strong contrast to the dopants investigated so far, MB is mainly located in the amorphous phase of P3HT leaving the structure of crystalline P3HT domains almost unaltered. Most remarkably, a very high charge conductivity of 3460 S/cm is obtained along the chain direction of P3HT with a resulting maximum power factor of 170±30 $\mu W/mK^2$. A comparative study on structure-property correlations in P3HT doped with different molecules (F_4TCNQ, $FeCl_3$, F_6TCNNQ and $Mo(tdf\text{-}COCF_3)_3$) highlights the way the dopant distribution in the semi-crystalline structure of P3HT determines the final charge transport and thermoelectric properties.

II. Results.

a) Anisotropic thermoelectric properties.

P3HT films were aligned by high-T rubbing at 186°C. A highly oriented semi-crystalline structure made of alternating crystalline lamellae and amorphous zones is thus obtained with a

total lamellar periodicity of 28 nm.[32,33] The lamellae are made of a majority of face-on crystals with some edge-on domains. Sequential doping of these films deposited on patterned substrates for conductivity measurements was performed with solutions of MB in acetonitrile (ACN) of increasing concentration for 40s-1min in a glove box. The Incremental Concentration Doping (ICS) of P3HT films leads to an improvement of TE properties based on a progressive intercalation of dopants in the pristine polymer structure as compared to direct doping using dopant solutions of high concentration.[18,19,31] The same oriented film was thus dipped in solutions of MB/ACN of increasing concentration [MB] and the anisotropic conductivity and Seebeck coefficient were measured along (//) and normal (⊥) to the rubbing direction (chain direction) (see Figure 1b-d).

Doping with [MB]≤0.05 g/l results in poor charge conductivities below 0.02 S/cm. Conductivity starts to increase for [MB]= 0.1 g/l and a record conductivity $\sigma_{//}$= 3460±600 S/cm is achieved for oriented P3HT doped with [MB]=0.2 g/l. Further doping of the films results in a slight reduction of the conductivity to 2900±300 S/cm for [MB]=1.0 g/l. The observed conductivity is much larger than that reported for non-oriented films doped in ambient conditions. As seen in figure S1, doping non-oriented P3HT films in a controlled atmosphere in a glove box already improves substantially the conductivity of the doped films by a factor of more than one order of magnitude (σ can reach up to 430 S/cm) as compared to films doped in ambient. This is consistent with previous reports for F_4TCNQ-doped P3HT.[31] However, orientation is necessary to increase charge conductivity to 3000 S/cm. The Seebeck coefficient decreases with increasing [MB] down to a value of 16±1 μV/K for 1.0 g/l parallel to the rubbing direction. As observed in previous studies, the Seebeck coefficient is larger along than perpendicular to the rubbing direction. In the direction perpendicular to the rubbing, $S_{\perp}$ reaching very small values of 3.5±0.5 μV/K for [MB]=1 g/l. The TE power factor PF shows accordingly a maximum for [MB]=0.2 g/l in the chain direction with $PF_{//}$=170±40

$\mu W/mK^2$. This value is comparable to the record value reported for oriented P3HT films doped with $Mo(tdf\text{-}CF_3)_3$ (160 $\mu W/mK^2$) (see Figure 1e-g). [23] These results are interesting and evidence a peculiar behavior when oriented P3HT films are doped with MB. Contrary to F_6TCNNQ, a saturation of the conductivity is reached at quite low doping concentration and in the case of MB, going to higher values of [MB] tends rather to decrease both conductivity and TE PF. Polarized UV-vis-NIR spectroscopy was used to clarify these trends *versus* [MB].

b) Polarons versus bipolaron spectroscopic signatures in MB-doped P3HT films.

Contrary to the conductivity showing important changes for [MB]≥0.2 g/l, the UV-vis-NIR spectra of oriented P3HT with POL//R evidences characteristic doping signatures at very low doping concentrations (0.05 g/l): i) the bleaching of the neutral P3HT absorption and ii) the appearance of polaronic bands P1 and P2 (see Figure 2). Accordingly, there is evidence for doping of crystalline P3HT domains. Evidence for a first isosbestic point at 650 nm between the neutral and P2 bands is found. For [MB]= 0.2 g/l, the neutral P3HT absorption is fully bleached. For higher [MB]=1.0 g/l, the presence of excess dopant on the film surface is manifested by an additional absorption peak at 703nm (band noted with a red asterisk in Figure 2). Very interesting is the situation observed for POL⊥R. The absorption band of amorphous interlamellar zones of P3HT at 500 nm shows also a bleaching upon doping. This effect was not observed when oriented P3HT films are doped with F_4TCNQ or F_6TCNNQ. As for the crystalline fraction of P3HT, the films doped with [MB]=0.2 g/l show a full bleaching of the absorption band of amorphous P3HT and the presence of well-defined polaronic bands P1 and P2. Both features indicate that MB dopes amorphous P3HT, in strong contrast to F_4TCNQ and F_6TCNNQ that cannot dope amorphous P3HT (the absorption of amorphous P3HT is unaffected by doping and no polaronic bands are seen for POL⊥R). Polarized UV-

vis-NIR spectroscopy indicates therefore that both oriented P3HT crystals and amorphous interlamellar zones are doped by MB.

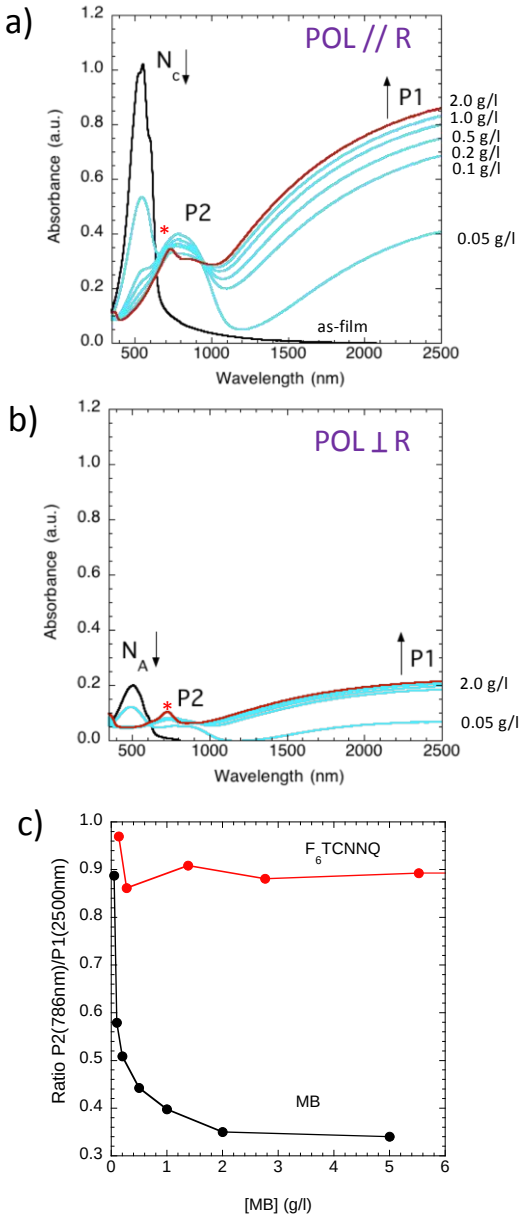

Figure 2. Evolution of the UV-vis-NIR spectra of oriented P3HT thin films (T_R=186°C) measured for light polarization (POL) oriented parallel (a) and perpendicular (b) to the chain direction. The red asterisk points at the absorption band of excess MB. N_a highlights the absorption band of amorphous P3HT whereas N_c corresponds to the absorption of neutral crystalline P3HT. P1 and P2 correspond to polaronic bands of doped P3HT. The spectra in black (red) correspond to undoped (doped, 2g/l) oriented P3HT. c) Evolution of the ratio r

between P2 and P1 band absorbances as a function of increasing [MB] and comparison with the result obtained for films doped with F_6TCNNQ (from reference 19).

The evolution of the UV-vis-NIR spectrum of oriented P3HT with increasing [MB] shows another marked difference with respect to the films doped with F_4TCNQ and F_6TCNNQ. This difference is obvious when plotting the ratio of the absorbances of the polaronic bands P2 at 700nm and P1 at 2500nm. In the case of MB, for [MB]≤ 0.1 g/l, the ratio r is close to 1 and identical to that observed for F_4TCNQ and F_6TCNNQ. This is characteristic of the presence of polarons in the doped polymers. However, r decreases and saturates to a value of 0.35 when doping with MB up to 5g/l whereas r remains unchanged whatever the doping concentration of F_6TCNNQ. Most interestingly, the UV-vis-NIR spectra show the existence of a second isosbestic point close to 947 nm between the P2 and the so-called P1 bands, suggesting that the polaronic specie formed at lower [MB] transforms into a different specie at higher doping concentration. This behavior is typical of the transformation of the polarons that are dominant for [MB]≤ 0.1 g/l into bipolarons for [MB]≥ 0.2 g/l. This observation is consistent with the results of Enengl et al. for P3HT films doped by electrochemical oxidation.[7] The increase of the oxidation potential of P3HT thin films leads to a similar decrease of the ratio r=P2/P1 and was attributed to a transformation of polarons into bipolarons as evidenced by Electron Spin Resonance. This interpretation is also consistent with the blue shift of the P1 band position with increasing dopant concentration (see Figure S2). Incidentally, the highest conductivity is observed in the oriented films of P3HT for [MB]=0.2g/l i.e. when the ratio P2/P1 is almost constant and the population of bipolarons is established. This result is similar to that reported by Neusser et al. on electrochemical doping of P3HT where the charge conductivity increases upon formation of bipolarons and reaches a plateau at high charge carrier concentration of $10^{21}cm^{-3}$. (8) Most importantly, when F_4TCNQ and F_6TCNNQ dope the only P3HT crystalline phase, no important population of bipolarons

is observed and the ratio P2/P1 is close to 1. Conversely, as demonstrated by TEM (vide infra), when the dopant is mainly located in the amorphous zones of P3HT, bipolaron formation is favored. In other words, the ratio of polaron and bipolaron absorption bands is *a priori* related to the preferential location of dopants in crystalline or amorphous phases of P3HT, respectively.

c) Determination of dopant concentration in thin films using RBS.

Further insight into the doping of P3HT with MB was obtained by Rutherford Back Scattering (RBS) that helps quantify the amount of MB present in the thin films (see Figures S3, S4 and table 1). For the P3HT films doped with MB, RBS can probe the presence of the dopant counterion $SbCl_6^-$ via Sb atoms *versus* sulfur atoms for P3HT (see Table 1). The atomic ratio Sb/S was determined for three samples doped at 0.2, 0.5 and 1.0 g/l (the samples doped at 0.5 and 1.0 g/l were doped at all lower concentrations following the ICD method). Regarding RBS data, we do observe an increase in the presence of Sb in the films when [MB] increases but the correlation between [MB] and Sb/S is not linear indicating that the doping is more effective at low [MB], in agreement with the charge conductivity measurements.

Table 1. Main thermoelectric properties of oriented P3HT thin films (T_R=186°C) doped with magic blue for different concentrations using the ICD method.

[MB] g/l	Sb/S atomic ratio (%)*	$\sigma_{//}$ (S/cm)	$\sigma_{\perp}$ (S/cm)	$S_{\perp}$ (S/cm)	$S_{//}$ (µV/K)	$PF_{//}$
0.2	6.7±0.4	3460±300	233±100	4.8	22	171
0.5	7.2+0.4	3250±400	213±150	4.1	18	167

1.0	10.2±0.6	2970±400	201±150	3.5	16	108

* measured by Rutherford Back Scattering.

Beside Sb and S, RBS identifies also the presence of Br in the thin films (see Figure S4). It can be associated to two species, namely excess of MB crystals on the film surface or to tris(4-bromophenyl)amine inside the P3HT films. Neither polarized optical microscopy, nor TEM reveal excess MB crystals in the thin films for [MB]≤0.5 g/l. Excess of MB crystals is visible only for [MB]≥1.0 g/l. This observation suggests that the presence of Br in the RBS spectra of doped P3HT is most likely due to tris(4-bromophenyl)amine present in the bulk of the doped P3HT thin films.

From the previous RBS measurements, we can determine the amount of ionized acceptor molecules N_A- assuming that all Sb atoms detected by RBS are present in the form of $SbCl_6^-$ counterions in the P3HT films. Moreover, if we assume that each counterion generates one free charge carrier, we can determine the density of holes N_p since $N_p = N_A$-. Knowing the unit cell volume of the doped P3HT (close to 1000 $Å^3$), we extract $N_p \approx 2.7 \cdot 10^{20}$ cm^{-3} for [MB]=0.2 g/l. This leads to an estimated lower bound value of the charge mobility in the direction of rubbing $\mu_{//} = 80$ $cm^2/V \cdot s$. As an alternative, we can also estimate the carrier density using the ratio P1/P2 and compare it with that observed by Neusser et al. for electrochemically doped P3HT. (8) From reference 8, one extracts a carrier density $N_p \approx 5 \cdot 10^{20}$ cm^{-3} leading to a charge mobility $\mu_{//} = 43$ $cm^2/V \cdot s$. This may suggest that RBS underestimates the amount of MB in the thin films, possibly because some MB sublimes upon prolonged exposure to high vacuum (see Figure S4). Both these values are substantially larger than for P3HT films doped with $Mo(tfd\text{-}CF_3)_3$ with $\mu_{//} = 7$ $cm^2/V \cdot s$ (N_p was determined using the absorbance of the polaronic band P2 measured by spectro-electrochemistry in a regime

dominated by polarons).[23] Worthy to mention, a band-like field effect mobility of 10 $cm^2/V{\cdot}s$ was recently reported for aligned PBTTT films in the crystalline phase doped with bis(trifluoromethylsulfonyl)imide.[34] To understand why the charge mobility can reach such high values in oriented P3HT films doped with MB, we studied the impact of MB doping on the structure of P3HT using transmission electron microscopy (electron diffraction).

d) Impact of doping on the structure of oriented P3HT probed by electron diffraction.

Electron diffraction is a simple means to follow the structural changes in aligned thin films of P3HT upon doping. Figure 3.a exemplifies the evolution of the ED pattern of oriented P3HT (T_R=186°C) as a function of the concentration of MB. Figure 3.b and 3.c collect the variations of d_{100} and π-stacking periodicity as a function of increasing dopant concentration for the five dopants investigated so far. From a general point of view, the ED pattern of MB-doped P3HT shows limited changes with increasing dopant concentration. Alignment is fully maintained upon doping whatever the concentration of doping. The π-stacking and d_{100} periodicities show virtually no change when the films are doped with MB (only a slight increase of d_{100} is seen at 0.2g/l) as compared to other dopants.

Previous studies have shown that dopant intercalation results in the expansion of the crystal lattice along the side chains of P3HT (**a** axis) and a contraction of the π-stacking distance. Such changes of crystal lattice are indeed well observed for the dopants F_4TCNQ, F_6TCNNQ, $FeCl_3$ and $Mo(tdf\text{-}COF_3)_3$ (see Figure 3 and Figure S5). Accordingly, the situation is clearly different for P3HT doped with MB. Doping of P3HT with MB leaves (h 0 2) reflections (h=0, 1, 2) almost unchanged in position and intensity even for high MB

concentrations. Previous studies have demonstrated that the evolution of the (h 0 2) reflections (h=0, 1, 2) with doping is a fingerprint of the dopant intercalation in the P3HT crystal lattice. [19,31] Intercalation of dopants inside P3HT crystals results in the disappearing of the 1 0 2 and 2 0 2 reflections and a streaking of the 0 0 2 reflection whose intensity increases substantially. These changes are the fingerprints of a re-organization of P3HT backbones within individual π-stacks. The recent structural refinement for F_6TCNNQ-doped P3HT has shown that doping P3HT with F_6TCNNQ induces a shift of P3HT backbones so as to group alkyl side chains and create cavities to host the dopant molecules in the crystal.[19]

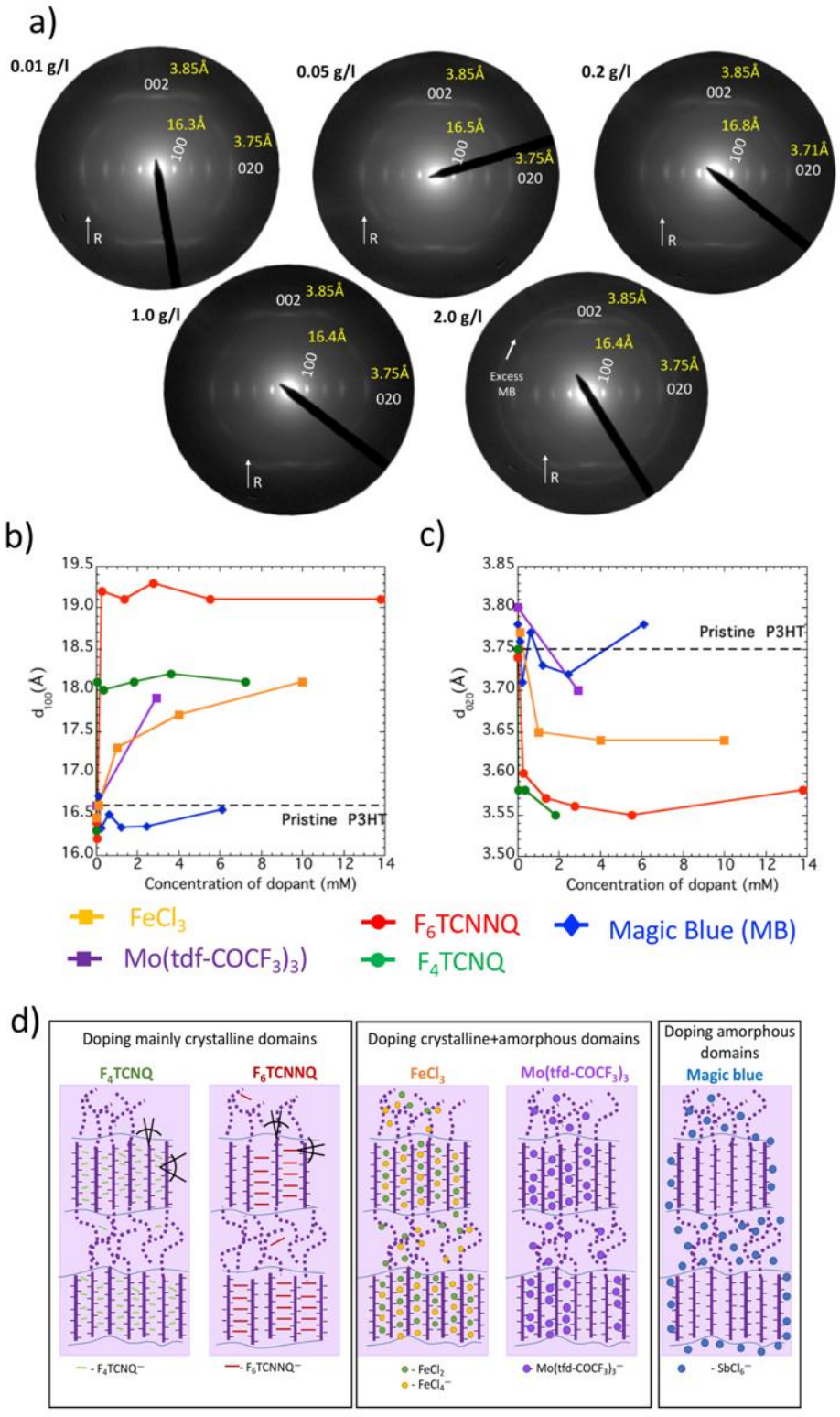

Figure 3. a) Structure evolution in oriented P3HT thin films doped with magic blue as obtained by low dose TEM. Electron diffraction patterns of doped P3HT film upon sequential doping with magic blue in acetonitrile from low to high doping concentration: The asterisk marks a Scherrer ring from excess magic blue on the surface of the doped P3HT film. R

represents the rubbing direction. b) and c) Evolution of the layer spacing along the alkyl side chain direction d_{100} (b) and the **π**-stacking periodicity d_{020} (c) as a function of the doping concentration for different dopants. The dotted lines highlight the values of the layer spacings d_{100} and d_{020} of undoped P3HT. d) Various doped P3HT microstructures: doping of the crystalline domains for F_4TCNQ and F_6TCNNQ; doping of both crystalline and amorphous zones for $FeCl_3$ and $Mo(tdf\text{-}COCF_3)_3$ and doping of the amorphous zones for Magic blue.

The present results demonstrates that doping with MB does not induce such a structural reorganization within π -stacks. There is thus evidence that MB is only marginally intercalated inside the P3HT lattice. Taken altogether, these results support the idea that doping of P3HT with MB leaves the crystal structure of P3HT mostly unchanged, contrary to all other investigated dopants (see Figure 3.d).

e) Doping kinetics for amorphous and crystalline P3HT.

Further understanding of the doping mechanism is gained by following the kinetics of doping by polarized UV-vis-NIR spectroscopy (see Figure 4). Working on oriented thin films helps investigate the doping kinetics for both crystalline and amorphous domains simply by selecting the incident light polarization. For POL//R, the UV-vis-NIR spectrum of rubbed P3HT films is dominated by the oriented crystalline fraction of P3HT and by the polaronic features P1 and P2 resulting from the doping (figure 4.a). For POL⊥R, the UV-vis-NIR spectra of pristine oriented films is dominated by the absorption of non-oriented and amorphous P3HT (Figure 4.b). Thus, by selecting the light polarization, one can choose to follow the apparent doping kinetics of either the crystalline or the amorphous fractions of P3HT. Our results show a very clear bleaching of the absorption bands of crystalline (POL//R) and amorphous POL⊥R) fractions with increasing doping time indicating that both

crystalline and amorphous P3HT domains are doped. In addition, the polaronic bands P1 and P2 are visible for both light polarizations, increasing in absorbance with increasing doping time and saturating after 1 min. To be more quantitative, we decided to probe the doping kinetics of both crystalline and amorphous P3HT phases by following the variation of the P1 absorbance at 2500 nm as a function of doping time for POL//R and POL⊥R (see Figure 4.c and 4.d). For the amorphous phase, the doping kinetics was also directly determined from the bleaching of the amorphous absorption peak near 500 nm (see Figure S6). Similar to our previous work, the doping kinetics can be adjusted using equation 1: [28]

$$A(t) = A_0(1 - \exp\left(-\frac{\sqrt{Dt}}{l}\right)) \qquad (1)$$

where A(t) is the absorption at wavelength 2500nm of the polaron at time t. A_0 is the absorbance of the polaron at saturation, ℓ is the film thickness and D is a fitting parameter that has the dimensions of a diffusion constant.

As a consequence, plotting the doping kinetics versus $\sqrt{t}/\ell$ leads to a representation that is independent on film thickness (see the doping kinetics for films of thickness 109 and 212 nm in Figure S7) and allows to extract the value of D for the two light polarizations (see Table 2).

From figure 4.c and 4.d, it turns out that the kinetics of both crystalline and amorphous zones are characterized by almost identical D values. In addition, the extracted values are remarkably close to the diffusion constant of iodine into P3HT i.e. 2.5 10^{-11} cm^2/s determined by Maliakal using attenuated total reflectance infrared (ATR-IR) spectroscopy.[35] It would therefore be tempting to claim that the similar values of D for POL//R and POL⊥R are due to similar diffusion coefficients of MB into amorphous and crystalline domains. However, TEM clearly shows that MB molecules do not enter the P3HT crystals even though spectroscopy demonstrates that they are doped. This apparent contradiction is solved by considering that the oriented P3HT crystals are doped from their interface with the surrounding amorphous

zones that contain MB molecules. Hence, the apparent doping kinetics observed for POL//R does not correspond to a diffusion kinetics of the dopants into P3HT crystals. It rather corresponds to the formation kinetics of polarons in P3HT crystals determined by the diffusion of MB into amorphous zones. This is why the fitting parameter D extracted for POL//R and POL⊥R are almost identical.

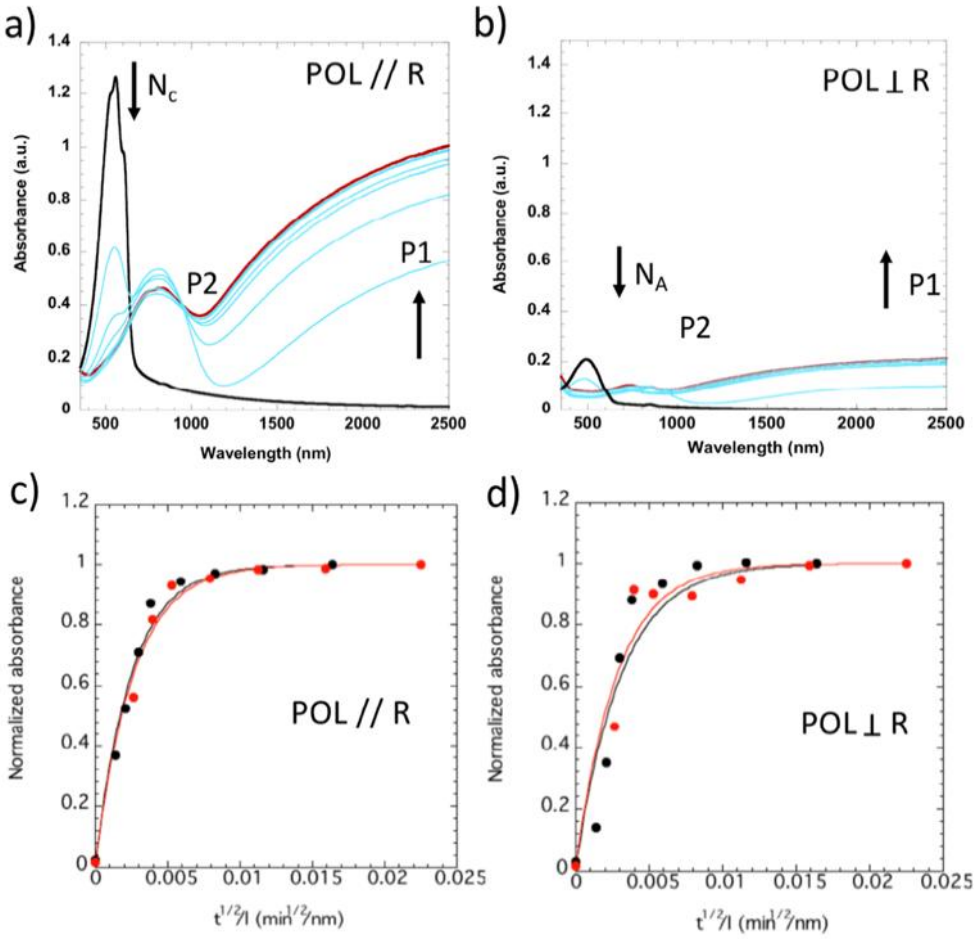

Figure 4. a) and b) Evolution of the UV-vis-NIR spectrum of oriented P3HT (T_R=186°C, thickness of 109±5 nm) with doping time for light polarized parallel (a) and perpendicular (b) to the polymer chain direction. N_C and N_A correspond to the absorbance of the neutral P3HT in crystalline and amorphous form, respectively. P1 and P2 refer to the polaronic absorption bands. c) and d) Evolution of the P1 absorbance at 2500nm as a function of √t/l with t the doping time and l the film thickness for oriented films of P3HT of thickness 109±5 nm (red

dots) and 212±11 nm (black dots) and for light polarized parallel (c) and perpendicular (d) to the polymer chain direction. The full lines in red and black correspond to the fits of the experimental data points using equation 1 (see text). The extracted doping constants are collected in table 2.

Table 2. Fitting parameter D (equation 1) describing the doping kinetics of oriented P3HT with MB observed with light polarized parallel (//) or perpendicular (⊥) to the P3HT chains.

Light polarization	Film thickness (nm)	D (cm^2/s) ($x10^{-11}$)
//	109±5	2.5±0.4
	212±11	2.8±0.3
⊥	109+5	2.2±0.6
	212±11	1.8±0.6

f) Correlations between Seebeck coefficient and charge conductivity in oriented semi-crystalline P3HT.

The S-σ correlations have been updated for the oriented P3HT thin films (see Figure 5). As highlighted in our previous work, there is a substantial difference in S-σ correlations measured parallel and normal to the chain direction, the former showing a power law dependence $S_{//} \propto \sigma^{-1/4}$ while the latter is logarithmic-like $S_{\perp} \propto -\ln(\sigma)$.[25,20] The power law dependence with an exponent s=-1/4 has been predicted by different models using either i) variable range hopping transport between localized states in a system with a gaussian DOS and Coulomb trapping by ionized dopants or ii) delocalized states such as Dirac fermions with a parabolic DOS and a scattering mechanism by unscreened charged impurities. (36,37) Gregory et al. proposed an improved version of the Kang and Snyder transport model i.e. a

semi-localized transport (SLoT) model to bridge the gap between localized and delocalized charge transport. (37,38) The domain of charge conductivity reached for the MB-doped P3HT suggests that a model involving rather delocalized states should be used to model transport in the chain direction, especially given the large carrier mobilities at play in this direction. For charge transport perpendicular to the P3HT chain direction, a model based on more localized states is certainly desired, but it has to follow a logarithmic dependence, not predicted by the previous models.

In the present contribution, we add the data points relative the films doped with MB. We observe that these additional data points help extend the S-σ correlation curve towards higher charge conductivities for both parallel and perpendicular directions to the polymer chain in P3HT. We notice also that the case of $FeCl_3$-doped films is peculiar in the high-concentration range as the conductivity drops off at a maximal conductivity of 580 S/cm contrary to MB-doped films.[20] Clearly, the link with structural data indicates that this "saturation" of $\sigma_{//}$ observed for $FeCl_3$ is due to the loss of crystalline order evidenced by TEM at high $FeCl_3$ concentration. No such effect is seen for MB-doped P3HT; the structure of P3HT is better preserved due to the selective doping of the amorphous phase. More generally, the scatter of S-σ data points for both parallel and perpendicular directions reflects the structural diversity in doped P3HT films i.e. the fact that different dopants can dope either crystalline, amorphous or both phases. In particular, the P3HT films doped with Mo(tdf-$COCF_3)_3$ stand out with respect to the other data points. In the chain direction, the fitting of the S-σ data points with a scaling law leads to a R-factor of 0.92 considering all data points and increases to 0.97 when excluding the points corresponding to Mo(tdf-$COCF_3)_3$ doped P3HT. Better-defined scaling laws have been observed for structurally more uniform materials such as PBTTT.[20,39] Therefore, beside the chemical nature of the dopants, the method of doping has a strong impact on the scaling laws. For instance, incremental

concentration doping or vapor phase doping that preserve better the pristine structure of the polymers than direct doping should help determine more accurately the S-σ correlations .[18-20]

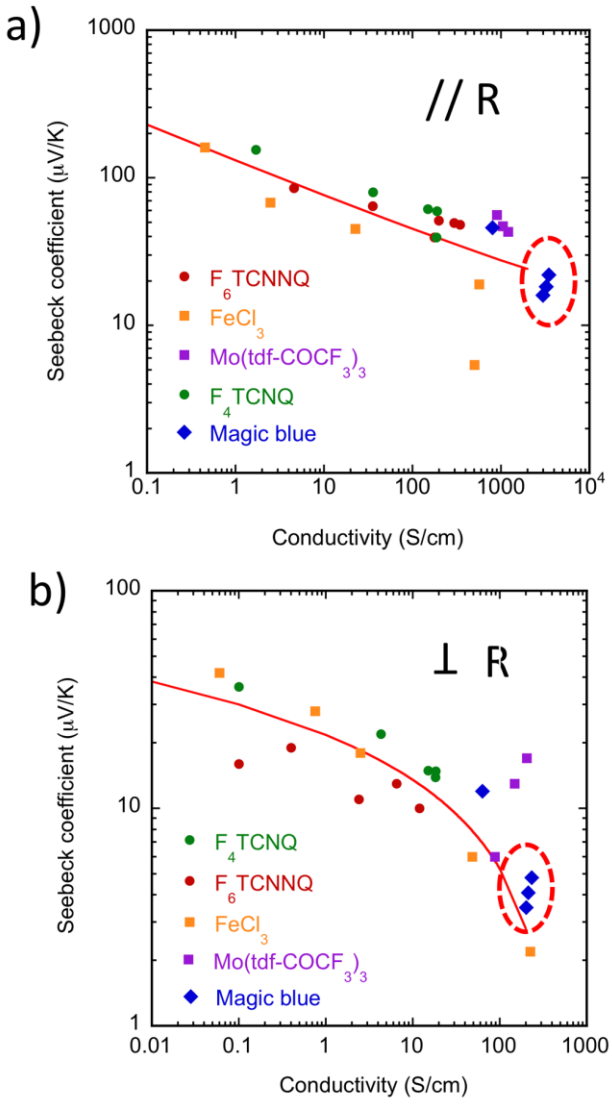

Figure 5. Correlations between Seebeck coefficient and charge conductivity probed parallel (a) and perpendicular (b) to the chain direction in thin films of P3HT oriented by high temperature rubbing at 186°C. The data correspond to thin films of P3HT doped sequentially with different dopants in acetonitrile (nitromethane for $FeCl_3$). The solid lines in a) and b) correspond to the result of a least-square fitting using a power-law ($\sigma_{//}$) or a log dependence ($\sigma_{\perp}$).

III. Discussion and conclusion.

A synoptic analysis of doping results obtained by TEM and polarized UV-vis-NIR spectroscopy in oriented P3HT thin films with various dopants helps identify three different situations illustrated in Figure 3.d. For dopants with $E_A \leq 5.4$ eV such as F_4TCNQ and F_6TCNNQ, doping of the only crystalline P3HT domains is observed because the electron affinity of the dopants is not sufficient to ensure charge transfer with the coiled P3HT chains present in the amorphous phase.[31] This is a clear-cut result from the polarized UV-vis-NIR spectroscopy showing that the absorption of amorphous P3HT is not at all bleached upon doping with these dopants. The consequence is that charge conductivity is rather limited in such systems with a maximum $\sigma_{//} = 520$ S/cm for F_6TCNNQ along the chain direction. TEM studies of the F_6TCNNQ-doped P3HT indicate that the doped phase of crystalline P3HT should have a stoichiometry of one F_6TCNNQ molecule per four thiophenes and a precise ordering of the dopant molecules within the crystal lattice of P3HT.[16] For stronger oxidants such as $FeCl_3$ and $Mo(tdf\text{-}COCF_3)_3$, both crystalline and amorphous phases are doped. Doping of amorphous P3HT domains is manifested in the polarized UV-vis-NIR spectra by the presence of the polaronic bands P1 and P2 for POL⊥R and bleaching of the absorption of amorphous P3HT. The lattice expansion probed by TEM shows that the unit cell expands along the **a**-axis up to 18.1 Å for $FeCl_3$ and 17.6 Å for $Mo(tdf\text{-}COCF_3)_3$. The highest charge conductivities reach a value of 570 S/cm, close to the values observed for films doped with F_6TCNNQ. For both these dopants, the increase of dopant concentration results in a saturation of the doping level evidenced by a saturation of the d_{100} value and of the absorbance of the polaronic bands. However, the diffraction patterns at high dopant concentration witness a substantial loss of packing order within P3HT crystals (loss of h 0 2 reflections and reduced intensity of the reflections).

The case of MB-doped P3HT films is clearly different. From the point of view of the film structure, TEM shows minor changes in lattice parameters and the overall ED patterns of P3HT remain almost unaltered upon doping. Despite unchanged crystal structure, polarized UV-vis-NIR spectroscopy demonstrates that the oriented crystalline phase of P3HT is doped and bipolarons are observed while record charge conductivities up to 3000 S/cm are measured. In parallel, an effective doping of the amorphous P3HT domains with MB is evidenced by UV-vis-NIR spectroscopy and the diffusion constants could be determined by UV-vis-NIR spectroscopy. This suggests that the P3HT nanocrystals must be doped via the surrounding amorphous/crystal interface and that the polarons can be delocalized inside the crystals. This last possibility would further imply that the distance between the polaronic charge and the counterions can be large, hence coulombic interactions can be reduced, explaining the larger mobility to the polarons delocalized in P3HT nanocrystals. *This rationale suggests that the preferential location of dopant molecules in the only amorphous domains of a semi-crystalline polymer semiconductor might be an effective strategy to reduce polaron localization through coulombic trapping by the dopant counterions. In other words, doping crystalline domains through the dopants in the surrounding amorphous phase is possibly a very effective way to drive the dopant counterions away from the polarons and to avoid charge carrier localization.*[40-42] It is important to further analyze which conditions in the choice of the polymer/dopant pair ensures such a situation. A priori, the EA of the dopant must be sufficiently high to dope readily amorphous areas of the polymer with a higher HOMO than crystalline regions. This is the case for dopants such as $FeCl_3$, $Mo(tdf\text{-}COCF_3)_3$ and MB. However, there is a marked difference between MB and these other two dopants since they are able to intercalate into P3HT crystals. The absence of MB molecules inside P3HT crystals as opposed to $FeCl_3$-doped films must somehow relate to the geometry and molecular dimensions of the dopants. The molecular volume of $SbCl_6^-$ (129 $Å^3$) is not

substantially larger than $FeCl_4^-$ (90 $Å^3$) or $FeCl_2$ and cannot explain the absence of MB in P3HT crystals. The latter species are very small and may diffuse readily in the crystals of P3HT. However, RBS results indicate that tris(4-bromophenyl)amine is present in the P3HT films doped with MB. Tris(4-bromophenyl)amine has a volume of 260 $Å^3$. If associated with $SbCl_6^-$ during diffusion, its substantially larger molecular volume in comparison to $FeCl_4^-$ should hinder effective diffusion into P3HT crystals and conversely promote the preferential location of MB into amorphous P3HT areas.

The case of P3HT/MB reminds PEDOT:PSS in various aspects such as i) the predominance of bipolarons as indicated by UV-vis-NIR spectroscopy, ii) the fact that counterions onto PSS chains surround the PEDOT nanocrystals and iii) the fact that so-called secondary crystallization induced by e.g. ethylene glycol helps to phase-separate PSS and PEDOT and hence improve the charge conductivity.[43,44] From this perspective, the intrinsic semi-crystalline nanostructuration of P3HT can be used as a scaffold for the selective nano-scale doping of the polymer.

IV. Experimental section

a) Orientation and doping of thin films: regio-regular P3HT was purchased from Merck (M_w = 43.6 kDa, PDI = 1.8). MB as well as anhydrous solvents (99%) used for doping (acetonitrile and nitromethane) and film preparation (ortho-dichlorobenzene) were purchased from Sigma Aldrich. The orientation of the films by high-T rubbing followed the protocol described in previous publications. [28,30] Rubbing is performed by using a homemade set-up consisting of a rotating cylinder covered with a microfiber cloth and a translating hot plate. The film thickness was extracted from the UV-vis absorbance using the calibration given in reference 23.

The doping of P3HT films with MB was performed following the incremental concentration doping (ICD) procedure[15,16] with full sample immersion for 40-60 s in the dopant solution of increasing concentration. The doped films were not rinsed with the pure solvent to avoid de-doping of the films. Both doping and rubbing were performed in a Jacomex glovebox.

b) Structural analysis by TEM. Oriented P3HT films were coated with a thin amorphous carbon film using an Edwards Auto306 evaporator. The films were removed from the glass substrate by floating on distilled water and recovered on TEM copper grids. A CM12 Philips microscope (120 kV) equipped with a MVIII (Soft Imaging System) charge coupled device camera TEM was used for the structural analysis of the films (bright field and diffraction modes). The 0 0 2 reflection at 3.85 Å is not sensitive to the doping of the polymer and was therefore used as an internal calibration to calculate the d_{100} and d_{020} reticular distances in the ED patterns. Beam exposure was set to a minimum using the low dose system to avoid de-doping under the electron beam when the same zone is exposed for a prolonged period of time. AFM was performed with a Multimode 8 Bruker with Nanoscope V controller using ScanAsyst-Air tips (0.4N/m). Cerius 2 software was used to calculate the molecular volumes of the dopant molecules.

c) Polarized UV–Vis–NIR absorption. A Varian Cary 5000 spectrometer with polarized incident light (spectral resolution of 1 nm) was used to probe the level of film orientation and the effect of film doping with MB (350–2500 nm) as a function of doping time and MB concentration. The angle of light polarization is measured with respect to the rubbing direction (0° corresponding to the light polarization POL//R and 90° corresponding to the light polarization POL⊥R).

d) Charge conductivity and Seebeck coefficient. All devices were fabricated on glass substrates cleaned by ultrasonication in acetone, ethanol, hellmanex and deionized water (x3 times). The cleaned substrates were dried under nitrogen and exposed to plasma prior to film deposition. Gold electrical contacts (40 nm thick) in a four-points probe geometry (1 mm spacing between electrodes, 5 mm length) were deposited via controlled thermal evaporation through a shadow mask, at an average rate of 4–6 Å/s. The geometry of gold electrodes allows to measure both the charge transport and thermopower on a same substrate in both parallel and perpendicular directions to the rubbing. Oriented films of P3HT were floated on water and carefully recovered on the device with pre-deposited gold electrodes. They were subsequently doped using the ICD protocol. [15,16]

All measurements of DC conductivity and Seebeck coefficients were performed in a Jacomex glovebox under N_2 atmosphere (< 1 ppm H_20 and < 2 ppm O_2). Four-point probe measurements of electrical conductivity were performed using a Keithley 4200-SCS and a Lab Assistant Semiprobe station. The resistivity ρ was derived from the sheet resistance R following the relation $\rho = 1.81 \cdot R \cdot t$ where t is the film thickness (the geometrical correction factor was determined following the method in reference 29). For each doping condition, two rubbed films deposited on substrates with four devices (2 oriented parallel and 2 oriented perpendicular to the rubbing) have been measured. The conductivity and Seebeck coefficients were calculated from the average resistance and the error from the standard variation. The film thickness was determined from the UV-vis absorbance using the calibration provided in references 23. A representative AFM image of an oriented 50nm-tick film is provided in figure S8.

The thermopower was measured using a differential temperature method whereby a temperature gradient was established across the sample along or perpendicular to the rubbing direction. The temperature gradient was ramped between 0 and 12K around room temperature

and the Seebeck coefficient was extracted by plotting the thermovoltage versus temperature gradient. A constantan wire was used to calibrate the Seebeck coefficient. The detailed procedure is given in references 29 and 31. All data were analyzed and fitted using Kaleidagraph program.

g) Rutherford backscattering method.

The Rutherford Backscattering Spectroscopy (RBS) measurements were performed on the 4 MV Van de Graaff accelerator of the ACACIA platform at ICube with a He^+ beam. An energy of 2 MeV and a scattering angle of 160 ° were chosen to have good mass separation of the various elements present in the layer. The probed area has a diameter of 800 μm. The statistical error on the determination of the elemental composition is 6%. To avoid local heating by the beam, a current of 3 nA was used. The incident beam was perpendicular to the surface of the sample.

Acknowledgments.

We thank the TEM platform from ICS for technical support. Christophe Contal is acknowledged for performing AFM measurements. Support from ANR through contract ANR -17-CE05-0012 (ANISOTHERM) and ANR-19-CE05-0036 (PSLM) is acknowledged. This work was financially supported by the European Commission through Marie Sklodowska-Curie project HORATES (GA-955837).

Conflict of interest.

The authors declare no conflicts of interest.

Data Availability Statement

The data that support the findings of this study are available from the corresponding author upon reasonable request.

References.

(1) K. Tremel and S. Ludwigs (2014) Morphology of P3HT in Thin Films in Relation to Optical and Electrical Properties. In: Ludwigs S. (eds) P3HT Revisited – From Molecular Scale to Solar Cell Devices. Advances in Polymer Science, vol. 265. Springer, Berlin, Heidelberg.

(2) P. C. Ewbank, M. C. Stefan, G. Sauvé, R. D. McCullough, Synthesis, Characterization and Properties of Regioregular Polythiophene-Based Materials. In *Handbook of Thiophene-Based Materials*; John Wiley & Sons, Ltd, 2009; pp 157–217.

(3) S. Ogawa, in *Organic Electronics*, Springer Japan, **2015**, pp 1-245.

(4) R. Kroon, R. D. A. Mengistie, D. Kiefer, J. Hynynen, J. D. Ryan, L. Yu, C. Müller, *Chem. Soc. Rev.* **2016**, *45*, 6147–6164.

(5) M. Goel, M. Thelakkat, *Macromolecules* **2020**, *53*, 3632–3642.

(6) A. D. Scaccabarozzi, A. Basu, F. Aniés, J. Liu, O. Zapata-Arteaga, R. Warren, Y. Firdaus, M. I. Nugraha, Y. Lin, M. Campoy-Quiles, N. Koch, C. Müller, L. Tsetseris, M. Heeney, T. D. Anthopoulos, *Chem. Rev.* **2021**. 122, 4420.

(7) C. Enengl, S. Enengl, S. Pluczyk, M. Havlicek, M. Lapkowski, H. Neugebauer, E. Ehrenfreund, *ChemPhysChem* **2016**, *17*, 3836.

(8) D. Neusser, C. Malacrida, M. Kern, Y. M. Gross, J. van Slageren, S. Ludwigs, *Chem. Mater.* **2020**, *32*, 6003.

(9) K. Bruchlos, D. Trefz, A. Hamidi-Sakr, M. Brinkmann, J. Heinze, A. Ruff, S. Ludwigs, *Electrochimica Acta* **2018**, *269*, 299.

(10) J. E. Cochran, M. J. N. Junk, A. M. Glaudell, P. L. Miller, J. S. Cowart, M. F. Toney, C. J. Hawker, B. F. Chmelka, M. L. Chabinyc, *Macromolecules* **2014**, *47*, 6836.

(11) Scholes D. Tyler, Yee Patrick Y., Lindemuth Jeffrey R., Kang Hyeyeon, Onorato Jonathan, Ghosh Raja, Luscombe Christine K., Spano Frank C., Tolbert Sarah H., Schwartz Benjamin J., *Adv. Funct. Mater.* **2017**, *27*, 1702654.

(12) D. T. Scholes, P. Y. Yee, G. R. McKeown, S. Li, H. Kang, J. R. Lindemuth, X. Xia, S. C. King, D. S. Seferos, S. H. Tolbert, B. J. Schwartz, *Chem. Mater.* **2019**, *31*, 73.

(13) D. T. Scholes, S. A. Hawks, P. Y. Yee, H. Wu, J. R. Lindemuth, S. H. Tolbert, B. J. Schwartz, *The Journal of Physical Chemistry Letters* **2015**, *6*, 4786.

(14) A. M. Glaudell, J. E. Cochran, S. N. Patel, M. L. Chabinyc, *Adv. Ener. Mater.* **2015**, *5* , 1401072.

(15) P. Pingel, and D. Neher, *Phys. Rev. B* **2013**, *87*, 115209.

(16) Y. Karpov, T. Erdmann, M. Stamm, U. Lappan, O. Guskova, M. Malanin, I. Raguzin, T. Beryozkina, V. Bakulev, F. Günther, S. Gemming, G. Seifert, M. Hambsch, S. Mannsfeld, B. Voit, A. Kiriy, *Macromolecules* **2017**, *50*, 914.

(17) M. Tietze, L. Burtone, M. Riede, B. Lüssem, B. and K. Leo, *Phys. Rev. B* **2012**, 86, 035320.

(18) V. Vijayakumar, P. Durand, H. Zeng, V. Untilova, L. Herrmann, P. Algayer, N. Leclerc, M. Brinkmann, *J. Mater. Chem. C* **2020**, *8*, 16470–16482.

(19) V. Untilova, H. Zeng, P. Durand, L. Herrmann, N. Leclerc, M. Brinkmann, *Macromolecules* **2021**, *54*, 6073.

(20) V. Vijayakumar, Y. Zhong, V. Untilova, M. Bahri, L. Herrmann, L. Biniek, N. Leclerc, M. Brinkmann, *Adv. Ener. Mater.* **2019**, *9*, 1900266.

(21) S. K. Mohapatra, Y. D. Zhang, B. Sandhu, M. S. Fonari, T. V. Timofeeva, S. R. Marder, S. Barlow, *Polyhedron* **2016,** *116*, 88-95.

(22) J. Hynynen, E. Järsvall, R. Kroon, Y. Zhang, S. Barlow, S. R. Marder, M. Kemerink, A. Lund, C. Müller, *ACS Macro Lett.* **2019**, *8*, 70.

(23) V. Untilova, J. Hynynen, A. I. Hofmann, D. Scheunemann, Y. Zhang, S. Barlow, M. Kemerink, S. R. Marder, L. Biniek, C. Müller, M. Brinkmann, *Macromolecules* **2020**, *53*, 6314.

(24) Z. Liang, Y. Zhang, M. Souri, X. Luo, A. M. Boehm, R. Li, Y. Zhang, T. Wang, D.-Y. Kim, J. Mei, S. R. Marder, K. R. Graham, *J. Mater. Chem. A* **2018**, *6*, 16495.

(25) A. M. Glaudell, J. E. Cochran, S. N. Patel, M. L. Chabinyc, *Adv. Ener. Mater.* **2015**, *5* , 1401072.

(26) S. N. Patel, A. M. Glaudell, K. A. Peterson, E. M. Thomas, K. A. O'Hara, E. Lim, M. L. Chabinyc, *Science Advances* **2017**, *3*.

(27) J. Hynynen, D. Kiefer, L. Yu, R. Kroon, R. Munir, A. Amassian, M. Kemerink, C. Müller, *Macromolecules* **2017**, *50* , 8140–8148.

(28) V. Vijayakumar, E. Zaborova, L. Biniek, H. Zeng, L. Herrmann, A. Carvalho, O. Boyron, N. Leclerc, M. Brinkmann, *ACS Appl. Mater. Interfaces* **2019**, *11*, 4942.

(29) A. Hamidi-Sakr, L. Biniek, J.-L. Bantignies, D. Maurin, L. Herrmann, N. Leclerc, P. Lévêque, V. Vijayakumar, N. Zimmermann, M. Brinkmann, *Adv. Funct. Mater.* **2017**, 27, 1700173.

(30) A. I. Hofmann, R. Kroon, S. Zokaei, E. Järsvall, C. Malacrida, S. Ludwigs, T. Biskup, C. Müller, *Adv. Elect. Mater.* **2020**, *6* , 2000249.

(31) V. Untilova, T. Biskup, L. Biniek, V. Vijayakumar, M. Brinkmann, *Macromolecules* **2020**, *53*, 2441–2453.

(32) M. Brinkmann and J.-C. Wittmann, *Adv. Mater.* **2006**, *18*, 860–863.

(33) A. Hamidi-Sakr, L. Biniek, S. Fall, M. Brinkmann, M. *Adv. Funct. Mater*., **2016**, *26*, 408–420.

(34) M. Ito, Y. Yamashita, T. Mori, K. Ariga, J. Takeya, and S. Watanabe, *Appl. Phys. Lett.* **2021,** *119*, 013302.

(35) A. J Maliakal, *ACS Appl. Mater. Interfaces* **2013**, *5* (17), 8300–8307.

(36) H. Abdalla,G. Zuo and M.Kemerink *Phys.Rev.B* **2017**, *96*,241202.

(37) M. Lepinoy, P. Limelette, B. Schmaltz, and F.T. Van, Scientific Reports **2020**, *10*, 8086.

(38) S. D. Kang, S. D. and G. J. Snyder, *Nat. Mater.* **2016**, 16, 252.

(39) D. Scheunemann, V. Vijayakumar, H. Zeng, P. Durand, N. Leclerc, M. Brinkmann, M. and M. Kemmerink, *Adv. elect. Mater.* **2020**, 6, 2000218.

(40) R. Ghosh, C. M. Pochas, and F. C. Spano, *J. Phys. Chem. C* **2016**, *120*, 11394.

(41) R. Ghosh, A. R. Chew, J. Onorato, V. Pakhnyuk, C. K. Luscombe, A. Salleo, F. C. Spano, *J. Phys. Chem. C* **2018**, 122, 18048–18060.

(42) A. R. Chew, R. Ghosh, Z. Shang, F. C. Spano, F. C. and A. Salleo, *J. Phys. Chem. Lett.* **2017**, 8, 4974.

(43) T. Takano, T.; H. Masunaga, A. Fujiwara, H. Okuzaki, and T. Sasaki, *Macromolecules*, **2012**, *4*5, 3859.

(44) N. Kim, S. Kee, S. L. Lee, B. H. Lee, Y. H. Kahng, Y. – R. Jo, B.-J. Kim, B.-J. and K. Lee, *Adv. Mater.* **2014**, 26, 2268.